Superconductivity modulated by structural phase transitions in pressurized vanadium-based kagome metals

Feng Du,[1,2,*] Rui Li,[1,2,*] Shuaishuai Luo,[1,2,*] Yu Gong,[3] Yanchun Li,[3] Sheng Jiang,[4] Brenden R. Ortiz,[5] Yi Liu,[6] Xiaofeng Xu,[6] Stephen D. Wilson,[5] Chao Cao,[1,2] Yu Song,[1,2,†] and Huiqiu Yuan[1,2,7,‡]

[1]*Center for Correlated Matter and Department of Physics, Zhejiang University, Hangzhou 310058, China*

[2]*Zhejiang Province Key Laboratory of Quantum Technology and Device, Department of Physics, Zhejiang University, Hangzhou 310058, China*

[3]*Beijing Synchrotron Radiation Facility, Institute of High Energy Physics, Chinese Academy of Sciences, Beijing 100049, China*

[4]*Shanghai Institute of Applied Physics, Chinese Academy of Sciences, Shanghai 201204, China*

[5]*Materials Department and California Nanosystems Institute, University of California Santa Barbara, Santa Barbara, California 93106, USA*

[6]*Key Laboratory of Quantum Precision Measurement of Zhejiang Province, Department of Applied Physics, Zhejiang University of Technology, Hangzhou 310023, China*

[7]*State Key Laboratory of Silicon Materials, Zhejiang University, Hangzhou 310058, China*

(Received 18 December 2021; revised 26 June 2022; accepted 11 July 2022; published 25 July 2022)

The interplay of superconductivity with electronic and structural instabilities on the kagome lattice provides a fertile ground for emergent phenomena. The vanadium-based kagome metals AV_3Sb_5 (A = K, Rb, Cs) exhibit superconductivity on an almost ideal kagome lattice, with the superconducting transition temperature T_c forming two domes upon pressure tuning. The first dome arises from the competition between superconductivity and a charge-density wave, whereas the origin for the second dome remains unclear. Herein, we show that the appearance of the second superconducting dome in KV_3Sb_5 and RbV_3Sb_5 is associated with transitions from hexagonal to monoclinic structures, evidenced by the splitting of structural peaks from synchrotron powder x-ray diffraction experiments and imaginary phonon frequencies in first-principles calculations. In KV_3Sb_5, the transition to an orthorhombic structure is further observed for pressure $p \gtrsim 20$ GPa, and is correlated with the strong suppression of T_c in the second superconducting dome. Our findings indicate that distortions of the crystal structure modulate superconductivity in AV_3Sb_5 under pressure, providing a platform to study kagome lattice superconductivity in the presence of multiple electronic and structural instabilities.

DOI: 10.1103/PhysRevB.106.024516

I. INTRODUCTION

The tuning of quantum materials provides a key for understanding their physics and a route towards potential applications. Highly tunable physical properties often emerge in the presence of electronic or structural instabilities, as seen in strongly correlated and two-dimensional materials [1–4]. Recently, kagome metals have come into focus because they natively harbor flat bands, saddle points, and topological electronic structures [5–9], fostering competing ground states and tunable physical properties. The kagome metals AV_3Sb_5 (A = K, Rb, Cs) [10–13] exhibit a giant anomalous Hall effect [14,15] in the absence of local magnetic moments [16], which may result from a chiral charge-density wave (CDW) that breaks time-reversal symmetry [17–21]. Moreover, superconductivity with evidence for a fully opened gap emerges at low temperatures [22–24] and raises the possibility of topological superconductivity [25,26].

As a clean and powerful tool that can be utilized to tailor materials atomic distances, and thus crystal and electronic structures, pressure is widely used to tune the properties of materials. The AV_3Sb_5 kagome metals are highly tunable by pressure or strain [27–37] and display a complex evolution of superconductivity with pressure. Under pressure, the CDW is quickly suppressed at $p_c \lesssim 2$ GPa, forming a superconducting dome with T_c maximized at p_c [28–30,34], consistent with competing CDW and superconductivity. More strikingly, a second superconducting dome is observed at higher pressures in all variants of AV_3Sb_5 [27,30–34]. While the origin for the second superconducting dome remains unsettled, proposals include a Liftshitz transition [31], the formation of a three-dimensional structural network via Sb-Sb bonding [38,39], and an interplay with magnetism [40]. Such two-dome superconductivity under pressure is rare, and highly nontrivial mechanisms are needed to account for its emergence. For instance, in $CeCu_2Si_2$, the two domes result from distinct superconducting pairing due to spin or valence fluctuations [41,42], and in iron chalcogenides they are tied to a change of the normal state from a Fermi liquid to a non-Fermi liquid [43,44]. Therefore, elucidating the underlying mechanism for the universal two-dome superconductivity under pressure is one of the key problems in the AV_3Sb_5

*These authors contributed equally to this work.
†yusong_phys@zju.edu.cn
‡hqyuan@zju.edu.cn

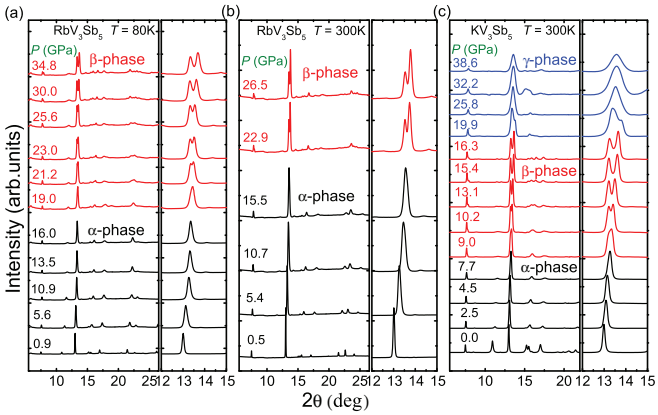

FIG. 1. XRD data under various pressures for (a) RbV_3Sb_5 at 80 K, (b) RbV_3Sb_5 at 300 K, and (c) KV_3Sb_5 at 300 K. The XRD patterns have been shifted vertically for clarity. The right side of each panel shows zoomed-in data, focusing on the peak near 13°. The colors of the diffraction patterns correspond to different structural phases, as indicated by the labels in the figure.

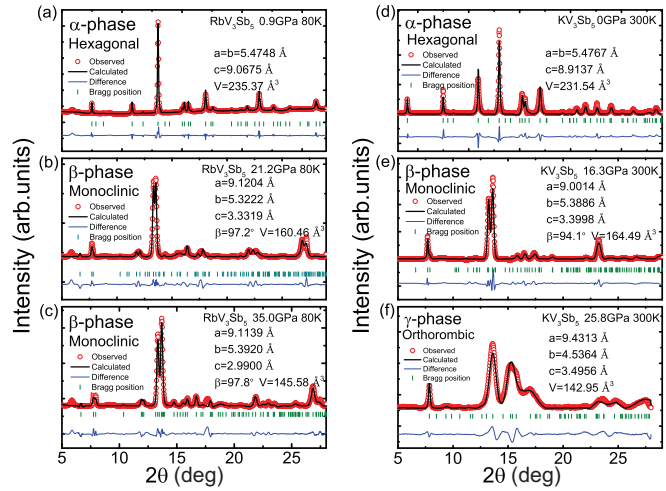

FIG. 2. XRD data for (a)–(c) RbV_3Sb_5 and (d)–(f) KV_3Sb_5 under various pressures. The diffraction data (open red circles) are fit to a hexagonal, a monoclinic, or an orthorhombic structure, using the Le Bail method.

series, the resolution of which could facilitate the understanding and engineering of these highly tunable kagome superconductors.

Here, combining synchrotron powder x-ray diffraction (XRD) and *ab initio* calculations, we show that transitions from hexagonal to monoclinic structures occur in both KV_3Sb_5 and RbV_3Sb_5. By comparing with resistivity measurements carried out using the same pressure medium, these structural transitions are identified to coincide with the appearance of the second superconducting dome in the two compounds. In KV_3Sb_5, another transition into an orthorhombic structure is observed upon further increase of pressure, whose emergence is associated with a strong suppression of T_c. These findings reveal pressure-induced structural modulations as a common origin for the emergence of the second superconducting dome in pressurized AV_3Sb_5 materials, and underscore structural instabilities as an integral aspect for understanding these vanadium-based kagome metals.

II. RESULTS

A. Powder x-ray diffraction under pressure

At ambient pressure, AV_3Sb_5 forms a hexagonal $P6/mmm$ structure above the CDW transition temperature, with a V kagome lattice interwoven with a Sb hexagonal lattice in the same layer, further encapsulated by layers of Sb (that form honeycomb lattices) above and below. These V_3Sb_5 slabs are well separated by alkaline metal ions, resulting in a highly two-dimensional structure. To investigate the stability of this structure under pressure and its relation to superconductivity, we carried out systematic powder XRD measurements under pressure. To facilitate a direct comparison with phase diagrams determined using resistivity [30,34], the same liquid pressure medium (silicon oil) is used in the XRD measurements. Experimental details are described in the Supplemental Material (SM) [45].

XRD data for RbV_3Sb_5 and KV_3Sb_5 under pressure are shown in Fig. 1 (see the SM for additional data on KV_3Sb_5 and RbV_3Sb_5 [45]). Diffraction patterns consistent with the ambient pressure hexagonal structure (α phase) are found to persist in RbV_3Sb_5 up to ≈16 GPa [Figs. 1(a) and 1(b)], and in KV_3Sb_5 up to ≈8 GPa [Fig. 1(c)]. Above these pressures, qualitative changes occur in the diffraction patterns; most prominently, the peak at ≈13° broadens and splits into two, with the split peak at larger scattering angles being more intense. The observation of such a splitting provides unequivocal evidence for a pressure-induced structural phase transition into a new phase (β phase). It is interesting to note that the splitting may become difficult to observe if the sample has prominent preferred orientations (see Fig. S1(b) in the SM for details [45]). The broadening first appears around 19.0 GPa in RbV_3Sb_5 [Fig. 1(a)] and around 9.0 GPa in KV_3Sb_5 [Fig. 1(c)], with the larger pressure in RbV_3Sb_5 consistent with the Rb atom's contribution to a negative chemical pressure. In addition, the evolution of the diffraction pattern for RbV_3Sb_5 at 300 K is consistent with that of 80 K, indicating that the pressure for the α-β phase transition does not vary strongly between the two temperatures.

While the β phase persists to the highest measured pressure in RbV_3Sb_5 (34.8 GPa), the split peaks merge into a single peak in KV_3Sb_5 for $p \gtrsim 20$ GPa (Fig. 1(c), and Fig. S1(a) in the SM [45]), signifying the appearance of a new structural phase (γ phase). At 19.9 GPa [Fig. 1(c)], even though two peaks are still present near 13°, the peak at smaller angles becomes more intense, distinct from scattering patterns of the β phase. On the other hand, the more intense peak of the two closely tracks the single peak in the γ phase. Therefore, the two peaks at 19.9 GPa can be understood to result from the sample being in a mixture of β and γ phases, which suggests that the transition is first-order-like and occurs close to 19.9 GPa.

To understand the nature of structural phases under pressure in RbV_3Sb_5 and KV_3Sb_5, the diffraction patterns are analyzed using the Le Bail method, with representative fits shown in Fig. 2. Peaks in the α phase can be indexed by

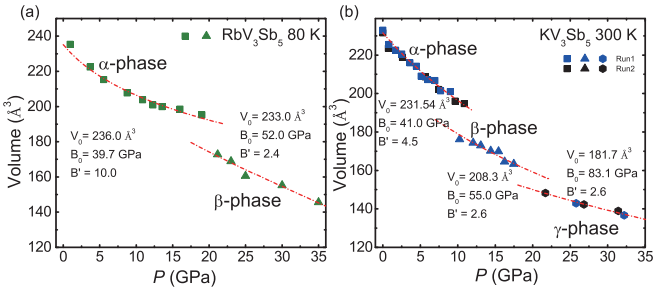

FIG. 3. The volume of the unit cell as a function of applied pressure for (a) RbV_3Sb_5 at 80 K, and (b) KV_3Sb_5 at 300 K. The dashed lines are fits to the Birch-Murnaghan equation of state (see the SM [45]), with corresponding parameters for different phases shown in the figure.

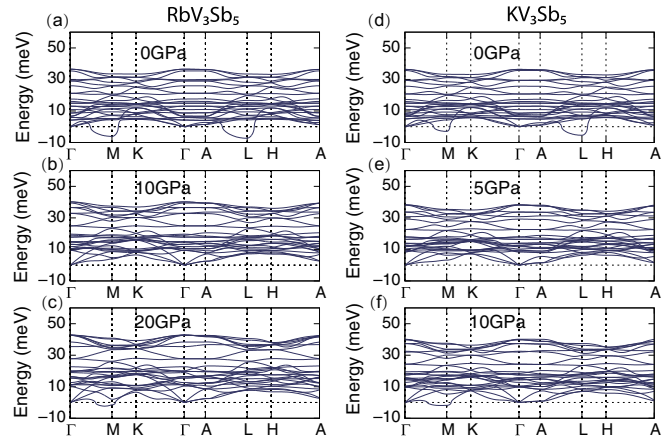

FIG. 4. (a)–(c) Calculated phonon spectra for RbV_3Sb_5 under various pressures. (d)–(f) Calculated phonon spectra for KV_3Sb_5 under various pressures.

the ambient pressure hexagonal $P6/mmm$ structure [Figs. 2(a) and 2(d)], with the intense peak around 13° corresponding to the in-plane Bragg peak (110). Diffraction patterns of the β phase can be described by a monoclinic structure [Figs. 2(b), 2(c), and 2(e)], which fully accounts for the split peaks around 13°, and are indexed as (020) and (011) of the monoclinic unit cell. For the γ phase of KV_3Sb_5, the diffraction patterns can be described by an orthorhombic structure [Fig. 2(f)], with a single intense (111) peak (indexed in the orthorhombic unit cell) around 13°. Lattice parameters for the α, β, and γ phases under representative pressures are shown in Fig. 2 (see the SM for the detailed evolution of the lattice parameters [45]). The systematic absences of Bragg peaks in the diffraction patterns constrain possible space groups for the β and γ phases, although space groups with identical selection rules cannot be distinguished. Based on the experimental data, the space group of the β phase could be $P2$, Pm, or $P2/m$, whereas the space group of the γ phase could be $P222$, $Pmm2$, or $Pmmm$.

The evolution of the unit cell volume with pressure is summarized in Fig. 3. Within each structural phase, pressure dependence of the unit cell volume is well described using the third-order Birch-Murnaghan equation of states (dashed lines in Fig. 3). On the other hand, a single set of parameters cannot describe the evolution of the unit cell volume over the entire measured pressure range, further corroborating the presence of distinct structural phases under pressure. A large ~9% volume reduction is observed across the α-β phase transition in both RbV_3Sb_5 and KV_3Sb_5, and a further ~6% volume reduction is seen across the β-γ phase transition in KV_3Sb_5.

B. First-principles calculations of phonon spectra

Motivated by the experimental evidence for pressure-induced structural phase transitions in RbV_3Sb_5 and KV_3Sb_5, their phonon spectra are calculated from first principles using a hexagonal $P6/mmm$ unit cell, with the results summarized in Fig. 4. The negative phonon frequencies in the plots indicate imaginary phonon modes, corresponding to structural instabilities. The reciprocal lattice vector and the symmetry classification of the lowest phonon mode can provide information on the ground-state crystal structure. At zero pressure, imaginary phonon modes are found at the M and L points in both RbV_3Sb_5 [Fig. 4(a)] and KV_3Sb_5 [Fig. 4(d)], with the leading instability at the L point. These phonon instabilities are B_{1u} modes, corresponding to a CDW state with a star-of-David (or its inverse) deformation of the kagome lattice [46], consistent with previous calculations for AV_3Sb_5 [40,47]. Increasing pressure to 10 GPa in RbV_3Sb_5 and 5 GPa in KV_3Sb_5 [Figs. 4(b) and 4(e)], the imaginary phonons associated with the CDW disappear, which indicates that the hexagonal $P6/mmm$ structure is stable at these pressures, consistent with the experimentally observed suppression of CDW above p_c ($\lesssim$2 GPa) [28–30,34].

With further increase of pressure, new imaginary phonon modes emerge around the M point in both RbV_3Sb_5 and KV_3Sb_5 [Figs. 4(c) and 4(f)], indicating the appearance of another structural instability. These instabilities are B_{3g} modes and are absent around the L point. Therefore, this structural instability is distinct from the CDW that occurs below p_c, and can instead be associated with the β phase uncovered in our XRD measurements. It is noteworthy that while 10 GPa is sufficient to induce this structural instability in KV_3Sb_5 [Fig. 4(f)], no imaginary phonon is found in RbV_3Sb_5 at the same pressure [Fig. 4(b)], consistent with the experimental observation that the β phase appears at a higher pressure in RbV_3Sb_5.

A previous first-principles study also found a second structural instability for CsV_3Sb_5 around 30–35 GPa, which is associated with a B_{1u} phonon mode, similar to the ambient pressure CDW [40]. The instability of the hexagonal structure found in our calculations for RbV_3Sb_5 and KV_3Sb_5 is different because (1) it is associated with a B_{3g} phonon mode, and (2) the instability of the hexagonal structure is not limited to a small pressure range, but persists to the highest pressures in our calculations (40 GPa for RbV_3Sb_5 and 30 GPa for KV_3Sb_5; see the SM for details [45]). Our first-principles calculations therefore point to a robust instability of the hexagonal structure in pressurized RbV_3Sb_5 and KV_3Sb_5, in contrast to the results from similar calculations for CsV_3Sb_5 under pressure [40], but consistent with our experimental XRD results.

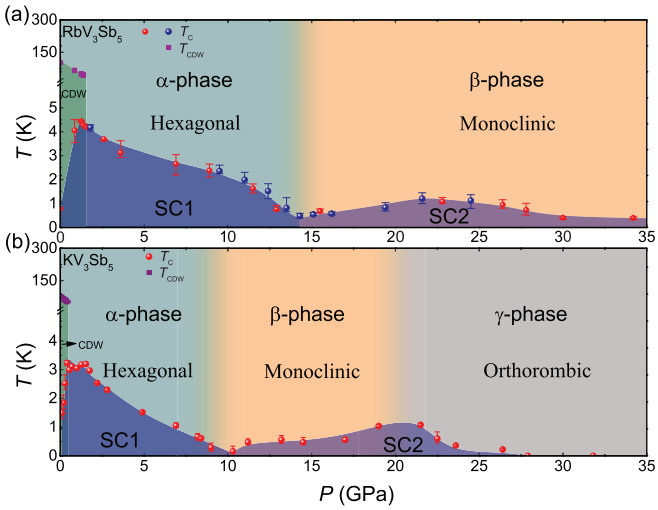

FIG. 5. (a) $P-T$ phase diagram for RbV_3Sb_5. (b) $P-T$ phase diagram for KV_3Sb_5. SC1 and SC2 correspond to the two superconducting domes revealed in transport measurements [30,34], with T_c for RbV_3Sb_5 obtained from measurements on two samples (shown as symbols in different colors). T_c and the CDW ordering temperature T_{CDW} for RbV_3Sb_5 are from Ref. [34], and those for KV_3Sb_5 are from Ref. [30]. The outlines of the superconducting domes are guides to the eye. Different structural phases are shaded in different colors. The β phase in RbV_3Sb_5 (300 K) first appears around 14.3 GPa (Fig. S2 in the SM [45]). The β phase in KV_3Sb_5 first appears around 9.0 GPa [Fig. 1(c)], and the γ phase first appears around 19.8 GPa (Fig. S1(a) in the SM [45]). The pressures in resistivity [30,34] and XRD measurements are both determined at room temperature, allowing for direct comparisons.

III. DISCUSSION AND CONCLUSION

Based on the XRD results in this work and previous resistivity measurements [30,34], the temperature-pressure phase diagrams for RbV_3Sb_5 and KV_3Sb_5 are constructed and shown in Fig. 5. As can be seen, the most striking feature in both RbV_3Sb_5 and KV_3Sb_5 is the observation of a structural transition from the α phase to the β phase, coinciding with or very close to a minimum in $T_c(p)$, which separates the two superconducting domes. In addition, the appearance of the γ phase in KV_3Sb_5 is accompanied by a suppression of T_c. Given our XRD experiments are carried out at 300 and 80 K, an important question is whether the pressure-induced α-β and β-γ phase transitions persist down to T_c. If the critical pressures for the α-β and β-γ transitions exhibit significant dependencies on temperature, then, close to the critical pressures, these transitions should also occur upon cooling and would lead to clear signatures in electrical transport, given that the α-β and β-γ phase transitions correspond to major changes in the crystal structure with distinct diffraction patterns. In previous measurements of electrical transport in pressurized RbV_3Sb_5 and KV_3Sb_5 [30,34], once the ambient pressure CDW is suppressed by applying pressure, there is only one resistive anomaly in electrical resistivity upon changing the temperature, occurring roughly around 200 K. This resistive anomaly (1) appears over a wide pressure range rather than limited to the vicinity of the critical pressures for the α-β and β-γ transitions, and (2) the diffraction patterns of the β phase RbV_3Sb_5 at 300 K and 80 K [Figs. 1(a) and 1(b)], which correspond to temperatures above and below this resistive anomaly, can be indexed by the same structure. Therefore, while the origin for the resistive anomaly in pressurized RbV_3Sb_5 and KV_3Sb_5 remains unclear, the two considerations above indicate that this resistive anomaly is not directly related to the α-β and β-γ transitions, and these pressure-induced structural transitions persist down to low temperatures, modulating superconductivity in RbV_3Sb_5 and KV_3Sb_5.

Due to difficulties in accurately obtaining diffraction peak intensities under pressure, Rietveld analysis cannot be carried out on our XRD data to precisely pin down the space group and the atomic coordinates of the β and γ phases. Nonetheless, insights on these structures can be gleaned by examining the structural evolution of related layered materials under pressure. Cold-pressed graphite is found to transition from a layered hexagonal structure to a monoclinic $C2/m$ or an orthorhombic $Pnma$ structure under pressure [48–50], with the formation of covalent bonds between distorted graphite layers. For 1T-TaS_2 under pressure, the layered hexagonal $P6_3/mmc$ structure first distorts, then interlayer S-S bonds form, and, finally, evolves into a tetragonal $I4/mmm$ structure [51], possibly via a monoclinic $C2/m$ intermediate phase [52]. A common theme in these materials is that the structures under ambient pressure are highly two dimensional and, with the application of pressure, interlayer bonds gradually form, before finally transitioning into a three-dimensional structure. These three-dimensional structures stabilized under pressure are often monoclinic, although orthorhombic or tetragonal structures may be close in energy. These considerations suggest that the β phase is likely a three-dimensional structure, with distorted kagome planes and interlayer Sb-Sb bonds, while the γ phase is close in energy, reminiscent of monoclinic and orthorhombic carbon [48–50]. This proposal is consistent with the dimensionality crossover observed in CsV_3Sb_5 under pressure [38,39], and also accounts for the large reduction in the unit cell volume across the α-β phase transition, which is likely dominated by a reduction in the interlayer atomic distances.

Given that the appearance of the second superconducting dome is accompanied by entrance into the β phase in both RbV_3Sb_5 and KV_3Sb_5, the transition between two structural phases is a natural candidate as the cause for two-dome superconductivity in these materials. In the case of CsV_3Sb_5, resistivity measurements suggest the presence of two superconducting domes, similar to RbV_3Sb_5 and KV_3Sb_5. However, powder XRD measurements at room temperature indicate that a hexagonal $P6/mmm$ structure (α phase) is adopted up to ≈80 GPa [39], seemingly different from our findings in RbV_3Sb_5 and KV_3Sb_5. Nonetheless, for pressures associated with the second superconducting dome, Raman scattering detected sharp changes in the zone-center optical phonons [29] and XRD measurements revealed the formation of interlayer Sb-Sb bonds [38,39], both already present at room temperature. Therefore, although CsV_3Sb_5 maintains a hexagonal $P6/mmm$ structure at room temperature up to 80 GPa, significant structural modulations occur under pressures associated with the second superconducting dome, despite persistence of the hexagonal structure under

pressure. Taken together with these findings in CsV_3Sb_5, our observations indicate that the second superconducting dome in pressurized AV_3Sb_5 results from pressure-induced lattice modulations.

The occurrence of the α-β transition demonstrates that superconductivity in the two superconducting domes of RbV_3Sb_5 and KV_3Sb_5 is associated with distinct structural phases, with an opposite evolution of T_c with pressure near the transition ($dT_c/dp < 0$ for the α phase and $dT_c/dp > 0$ for the β phase). While the superconducting pairing mechanism of AV_3Sb_5 remains unsettled, for electron-phonon pairing such a change in the sign of dT_c/dp across the α-β transition may result from sudden changes in the density of states at the Fermi level, the Debye frequency, or the electron-phonon coupling. Within the second superconducting dome, a further mechanism is needed to account for the nonmonotonic evolution of T_c with pressure that gives rise to the dome of superconductivity. In the case of KV_3Sb_5, the strong suppression of T_c for $p \gtrsim 20$ GPa in the second superconducting dome is clearly associated with the γ phase [Fig. 5(b)]. On the other hand, the mechanism for the broader superconducting domes in RbV_3Sb_5 [Fig. 5(a)] and CsV_3Sb_5 remains to be investigated. Within an electron-phonon pairing mechanism, such a domelike pressure dependence of T_c could arise when the Debye frequency and the density of states at the Fermi level exhibit an opposite evolution under pressure. In addition, possible connections between resistivity anomalies in the normal state [30,34] and the second superconducting dome warrant further studies.

In conclusion, we systematically investigated the evolution of RbV_3Sb_5 and KV_3Sb_5 under pressure using powder x-ray diffraction and first-principles calculations, and uncovered a transition into a distinct structural phase upon increasing pressure. Compared against resistivity measurements obtained using the same pressure medium, we find that the structural transition occurs around a minimum in $T_c(p)$, and naturally accounts for the presence of two superconducting domes in these materials. In KV_3Sb_5, an additional structural phase transition is found at higher pressures, which is associated with a strong suppression of superconductivity in the second superconducting dome. These findings demonstrate that in addition to electronic instabilities on the kagome lattice, structural instabilities play an integral role in the complex evolution of superconductivity in pressurized AV_3Sb_5, and suggest a potential role of the corresponding soft phonons in determining their physical properties under ambient pressure.

ACKNOWLEDGMENTS

We acknowledge Zhongyi Lu for helpful discussions and Guanghan Cao for assistance in sample preparation. This work was supported by the National Key R&D Program of China (Grants No. 2017YFA0303100, No. 2016YFA0300202, and No. 2017YFA0403401), the Key R&D Program of Zhejiang Province, China (Grant No. 2021C01002), the National Natural Science Foundation of China (Grants No. 12034017, No. 11974306, No. 11874137, and No. 11974061), and the Fundamental Research Funds for the Central Universities of China. S.D.W. and B.R.O. gratefully acknowledge support via the University of California Santa Barbara NSF Quantum Foundry funded via the Q-AMASE-i program under Award No. DMR-1906325. B.R.O. also acknowledges support from the California NanoSystems Institute through the Elings fellowship program.

[1] B. Keimer, S. A. Kivelson, M. R. Norman, S. Uchida, and J. Zaanen, Nature (London) **518**, 179 (2015).
[2] Q. Si and F. Steglich, Science **329**, 1161 (2010).
[3] T. Shibauchi, A. Carrington, and Y. Matsuda, Annu. Rev. Condens. Matter Phys. **5**, 113 (2014).
[4] Y. Cao, V. Fatemi, S. Fang, K. Watanabe, T. Taniguchi, E. Kaxiras, and P. Jarillo-Herrero, Nature (London) **556**, 43 (2018).
[5] H.-M. Guo and M. Franz, Phys. Rev. B **80**, 113102 (2009).
[6] I. I. Mazin, H. O. Jeschke, F. Lechermann, H. Lee, M. Fink, R. Thomale, and R. Valentí, Nat. Commun. **5**, 4261 (2014).
[7] L. Ye, M. Kang, J. Liu, F. von Cube, C. R. Wicker, T. Suzuki, C. Jozwiak, A. Bostwick, E. Rotenberg, D. C. Bell, L. Fu, R. Comin, and J. G. Checkelsky, Nature (London) **555**, 638 (2018).
[8] E. Liu, Y. Sun, N. Kumar, L. Muechler, A. Sun, L. Jiao, S.-Y. Yang, D. Liu, A. Liang, Q. Xu, J. Kroder, V. Süß, H. Borrmann, C. Shekhar, Z. Wang, C. Xi, W. Wang, W. Schnelle, S. Wirth, Y. Chen *et al.*, Nat. Phys. **14**, 1125 (2018).
[9] M. Kang, L. Ye, S. Fang, J.-S. You, A. Levitan, M. Han, J. I. Facio, C. Jozwiak, A. Bostwick, E. Rotenberg, M. K. Chan, R. D. McDonald, D. Graf, K. Kaznatcheev, E. Vescovo, D. C. Bell, E. Kaxiras, J. van den Brink, M. Richter, M. P. Ghimire *et al.*, Nat. Mater. **19**, 163 (2020).
[10] B. R. Ortiz, L. C. Gomes, J. R. Morey, M. Winiarski, M. Bordelon, J. S. Mangum, I. W. H. Oswald, J. A. Rodriguez-Rivera, J. R. Neilson, S. D. Wilson, E. Ertekin, T. M. McQueen, and E. S. Toberer, Phys. Rev. Mater. **3**, 094407 (2019).
[11] B. R. Ortiz, S. M. L. Teicher, Y. Hu, J. L. Zuo, P. M. Sarte, E. C. Schueller, A. M. Milinda Abeykoon, M. J. Krogstad, S. Rosenkranz, R. Osborn, R. Seshadri, L. Balents, J. He, and S. D. Wilson, Phys. Rev. Lett. **125**, 247002 (2020).
[12] Q. Yin, Z. Tu, C. Gong, Y. Fu, S. Yan, and H. Lei, Chin. Phys. Lett. **38**, 037403 (2021).
[13] B. R. Ortiz, P. M. Sarte, E. M. Kenney, M. J. Graf, S. M. L. Teicher, R. Seshadri, and S. D. Wilson, Phys. Rev. Mater. **5**, 034801 (2021).
[14] S.-Y. Yang, Y. Wang, B. R. Ortiz, D. Liu, J. Gayles, E. Derunova, R. Gonzalez-Hernandez, L. Šmejkal, Y. Chen, S. S. P. Parkin, S. D. Wilson, E. S. Toberer, T. McQueen, and M. N. Ali, Sci. Adv. **6**, eabb6003 (2020).
[15] F. H. Yu, T. Wu, Z. Y. Wang, B. Lei, W. Z. Zhuo, J. J. Ying, and X. H. Chen, Phys. Rev. B **104**, L041103 (2021).
[16] E. M. Kenney, B. R. Ortiz, C. Wang, S. D. Wilson, and M. J. Graf, J. Phys.: Condens. Matter **33**, 235801 (2021).
[17] Y.-X. Jiang, J.-X. Yin, M. M. Denner, N. Shumiya, B. R. Ortiz, G. Xu, Z. Guguchia, J. He, M. S. Hossain, X. Liu, J. Ruff, L. Kautzsch, S. S. Zhang, G. Chang, I. Belopolski, Q. Zhang,

T. A. Cochran, D. Multer, M. Litskevich, Z.-J. Cheng *et al.*, Nat. Mater. **20**, 1353 (2021).
[18] X. Feng, K. Jiang, Z. Wang, and J. Hu, Sci. Bull. **66**, 1384 (2021).
[19] C. Mielke III, D. Das, J.-X. Yin, H. Liu, R. Gupta, Y.-X. Jiang, M. Medarde, X. Wu, H. C. Lei, J. Chang, P. Dai, Q. Si, H. Miao, R. Thomale, T. Neupert, Y. Shi, R. Khasanov, M. Z. Hasan, H. Luetkens, and Z. Guguchia, Nature (London) **602**, 245 (2022).
[20] L. Yu, C. Wang, Y. Zhang, M. Sander, S. Ni, Z. Lu, S. Ma, Z. Wang, Z. Zhao, H. Chen, K. Jiang, Y. Zhang, H. Yang, F. Zhou, X. Dong, S. L. Johnson, M. J. Graf, J. Hu, H.-J. Gao, and Z. Zhao, arXiv:2107.10714.
[21] C. Setty, H. Hu, L. Chen, and Q. Si, arXiv:2105.15204.
[22] W. Duan, Z. Nie, S. Luo, F. Yu, B. R. Ortiz, L. Yin, H. Su, F. Du, A. Wang, Y. Chen, X. Lu, J. Ying, S. D. Wilson, X. Chen, Y. Song, and H. Yuan, Sci. China Phys. Mech. Astron. **64**, 107462 (2021).
[23] C. Mu, Q. Yin, Z. Tu, C. Gong, H. Lei, Z. Li, and J. Luo, Chin. Phys. Lett. **38**, 077402 (2021).
[24] H.-S. Xu, Y.-J. Yan, R. Yin, W. Xia, S. Fang, Z. Chen, Y. Li, W. Yang, Y. Guo, and D.-L. Feng, Phys. Rev. Lett. **127**, 187004 (2021).
[25] Y. Wang, S. Yang, P. K. Sivakumar, B. R. Ortiz, S. M. L. Teicher, H. Wu, A. K. Srivastava, C. Garg, D. Liu, S. S. P. Parkin, E. S. Toberer, T. McQueen, S. D. Wilson, and M. N. Ali, arXiv:2012.05898.
[26] Z. Liang, X. Hou, F. Zhang, W. Ma, P. Wu, Z. Zhang, F. Yu, J.-J. Ying, K. Jiang, L. Shan, Z. Wang, and X.-H. Chen, Phys. Rev. X **11**, 031026 (2021).
[27] C. C. Zhao, L. S. Wang, W. Xia, Q. W. Yin, J. M. Ni, Y. Y. Huang, C. P. Tu, Z. C. Tao, Z. J. Tu, C. S. Gong, H. C. Lei, Y. F. Guo, X. F. Yang, and S. Y. Li, arXiv:2102.08356.
[28] F. H. Yu, D. H. Ma, W. Z. Zhuo, S. Q. Liu, X. K. Wen, B. Lei, J. J. Ying, and X. H. Chen, Nat. Commun. **12**, 3645 (2021).
[29] K. Y. Chen, N. N. Wang, Q. W. Yin, Y. H. Gu, K. Jiang, Z. J. Tu, C. S. Gong, Y. Uwatoko, J. P. Sun, H. C. Lei, J. P. Hu, and J.-G. Cheng, Phys. Rev. Lett. **126**, 247001 (2021).
[30] F. Du, S. Luo, B. R. Ortiz, Y. Chen, W. Duan, D. Zhang, X. Lu, S. D. Wilson, Y. Song, and H. Yuan, Phys. Rev. B **103**, L220504 (2021).
[31] X. Chen, X. Zhan, X. Wang, J. Deng, X.-B. Liu, X. Chen, J.-G. Guo, and X. Chen, Chin. Phys. Lett. **38**, 057402 (2021).
[32] Z. Zhang, Z. Chen, Y. Zhou, Y. Yuan, S. Wang, J. Wang, H. Yang, C. An, L. Zhang, X. Zhu, Y. Zhou, X. Chen, J. Zhou, and Z. Yang, Phys. Rev. B **103**, 224513 (2021).
[33] C. C. Zhu, X. F. Yang, W. Xia, Q. W. Yin, L. S. Wang, C. C. Zhao, D. Z. Dai, C. P. Tu, B. Q. Song, Z. C. Tao, Z. J. Tu, C. S. Gong, H. C. Lei, Y. F. Guo, and S. Y. Li, Phys. Rev. B **105**, 094507 (2022).
[34] F. Du, S. Luo, R. Li, B. R. Ortiz, Y. Chen, S. D. Wilson, Y. Song, and H. Yuan, Chin. Phys. B **31**, 017404 (2022).
[35] L. Yin, D. Zhang, C. Chen, G. Ye, F. Yu, B. R. Ortiz, S. Luo, W. Duan, H. Su, J. Ying, S. D. Wilson, X. Chen, H. Yuan, Y. Song, and X. Lu, Phys. Rev. B **104**, 174507 (2021).
[36] B. Q. Song, X. M. Kong, W. Xia, Q. W. Yin, C. P. Tu, C. C. Zhao, D. Z. Dai, K. Meng, Z. C. Tao, Z. J. Tu, C. S. Gong, H. C. Lei, Y. F. Guo, X. F. Yang, and S. Y. Li, arXiv:2105.09248.
[37] T. Qian, M. H. Christensen, C. Hu, A. Saha, B. M. Andersen, R. M. Fernandes, T. Birol, and N. Ni, Phys. Rev. B **104**, 144506 (2021).
[38] A. Tsirlin, P. Fertey, B. R. Ortiz, B. Klis, V. Merkl, M. Dressel, S. Wilson, and E. Uykur, Sci. Post Phys. **12**, 049 (2022).
[39] F. Yu, X. Zhu, X. Wen, Z. Gui, Z. Li, Y. Han, T. Wu, Z. Wang, Z. Xiang, Z. Qiao, J. Ying, and X. Chen, Phys. Rev. Lett. **128**, 077001 (2022).
[40] J.-F. Zhang, K. Liu, and Z.-Y. Lu, Phys. Rev. B **104**, 195130 (2021).
[41] H. Q. Yuan, F. M. Grosche, M. Deppe, C. Geibel, G. Sparn, and F. Steglich, Science **302**, 2104 (2003).
[42] H. Q. Yuan, F. M. Grosche, M. Deppe, G. Sparn, C. Geibel, and F. Steglich, Phys. Rev. Lett. **96**, 047008 (2006).
[43] L. Sun, X.-J. Chen, J. Guo, P. Gao, Q.-Z. Huang, H. Wang, M. Fang, X. Chen, G. Chen, Q. Wu, C. Zhang, D. Gu, X. Dong, L. Wang, K. Yang, A. Li, X. Dai, H. kwang Mao, and Z. Zhao, Nature (London) **483**, 67 (2012).
[44] J. P. Sun, P. Shahi, H. X. Zhou, Y. L. Huang, K. Y. Chen, B. S. Wang, S. L. Ni, N. N. Li, K. Zhang, W. G. Yang, Y. Uwatoko, G. Xing, J. Sun, D. J. Singh, K. Jin, F. Zhou, G. M. Zhang, X. L. Dong, Z. X. Zhao, and J.-G. Cheng, Nat. Commun. **9**, 380 (2018).
[45] See Supplemental Material at http://link.aps.org/supplemental/10.1103/PhysRevB.106.024516 for information on experimental details, first-principles phonon calculations, additional experimental data and calculated phonon spectra, and evolution of the lattice parameters under pressure.
[46] B. R. Ortiz, S. M. L. Teicher, L. Kautzsch, P. M. Sarte, N. Ratcliff, J. Harter, J. P. C. Ruff, R. Seshadri, and S. D. Wilson, Phys. Rev. X **11**, 041030 (2021).
[47] H. Tan, Y. Liu, Z. Wang, and B. Yan, Phys. Rev. Lett. **127**, 046401 (2021).
[48] Q. Li, Y. Ma, A. R. Oganov, H. Wang, H. Wang, Y. Xu, T. Cui, H.-K. Mao, and G. Zou, Phys. Rev. Lett. **102**, 175506 (2009).
[49] J.-T. Wang, C. Chen, and Y. Kawazoe, Phys. Rev. Lett. **106**, 075501 (2011).
[50] Y. Wang, J. E. Panzik, B. Kiefer, and K. K. M. Lee, Sci. Rep. **2**, 520 (2012).
[51] Q. Dong, Q. Li, S. Li, X. Shi, S. Niu, S. Liu, R. Liu, B. Liu, X. Luo, J. Si, W. Lu, N. Hao, Y. Sun, and B. Liu, npj Quantum Mater. **6**, 20 (2021).
[52] X. Wang, Y. Liu, X. Chen, P. Zhang, and X. Liu, Phys. Chem. Chem. Phys. **22**, 8827 (2020).